Cement & Concrete Composites 31 (2009) 682–691

Contents lists available at ScienceDirect

Cement & Concrete Composites

journal homepage: www.elsevier.com/locate/cemconcomp

Ductility analysis of compression-yielding FRP-reinforced composite beams

Y.W. Zhou [a,b], Y.F. Wu [a,*], J.G. Teng [c], A.Y.T. Leung [a]

[a] Department of Building and Construction, City University of Hong Kong, Hong Kong, China
[b] School of Civil and Hydraulic Engineering, Dalian University of Technology, Dalian, China
[c] Department of Civil and Structural Engineering, The Hong Kong Polytechnic University, Hong Kong, China

ARTICLE INFO

Article history:
Received 13 January 2008
Received in revised form 23 June 2009
Accepted 27 June 2009
Available online 1 July 2009

Keywords:
Ductility
Compression yielding
FRP
Concrete beams
Numerical simulation
Analytical study

ABSTRACT

Ductility is one of the major issues of concern in achieving the widespread acceptance of FRP-reinforced concrete structures in practice. A new technique for improving the ductility of FRP-reinforced concrete beams through compression yielding (CY) instead of tensile yielding in the plastic hinge zone has recently been developed. A CY beam is a relatively complicated composite member that incorporates an additional composite material into the plastic hinge of a FRP-reinforced concrete beam. This paper presents the results of an investigation into the ductility behavior of CY beams. Results from a numerical study are first presented to illustrate the effects of key variables on the ductility performance of CY beams. These effects are then comprehensively examined through an analytical study. Finally, general conclusions on the ductility design of CY beams are provided.

1. Introduction

During the past decade, FRP-reinforced concrete structures have attracted world-wide interest in both application and research [1–3]. However, FRP is a brittle material and will rupture suddenly when loaded beyond its tensile strength, without providing ductility. Therefore, the ductility of FRP-reinforced concrete structures has become a major concern [4,5]. To address this concern, a new concept of achieving ductility through compression yielding (CY) has recently been introduced [6–11]. In a CY beam, a CY block is placed on the compression side of the member in the plastic hinge zone to replace concrete, as shown in Fig. 1. The ductility of a CY beam is achieved through the compression yielding of the CY block instead of the tensile yielding of the reinforcing bars. As the plastic deformation of a CY beam is concentrated in the plastic hinge zone of a member, a large amount of ductility is usually demanded of the CY block. Two effective approaches for meeting this high ductility demand of the CY block have been developed. One is through the use of a special ductile material, such as perforated SIFCON blocks [10]; the other is through the use of a ductile steel mechanism [11]. Laboratory testing has demonstrated the use of a CY block to be highly effective in increasing the ductility of FRP-reinforced concrete beams [6–8,10].

The configuration of a typical CY beam is shown in Fig. 1. The CY block is prefabricated with starter bars that will be lapped with the normal hanger or compression bars of the cast in situ concrete. Therefore, the plastic hinge of a CY beam is composed of four materials: FRP reinforcement, cast in situ concrete, a precast CY block, and the compression steel bars (that may be omitted) passing through the CY block. The ductility of a CY beam is directly related to the ductility of the plastic hinge and this relationship has previously been derived [7]. As a result, to examine the ductility of a CY beam, it is only necessary to study the ductility of the plastic hinge. Therefore this work focuses on the effects of CY material properties on the moment–curvature response of the plastic hinge of a CY beam.

In this study, the CY block material is assumed to be elastic-perfectly plastic [7], as shown in Fig. 2. For such a CY beam with a given cross-section and fixed material properties for the steel and the FRP reinforcement, the cross-sectional behavior of the plastic hinge is governed by only six parameters (or variables): the height of the CY block ηd, the strength f_b, the yield strain ε_{by} (or the elastic modulus E_b) and the ultimate strain ε_{bu} of the CY material, the compression reinforcement ratio ρ_s, and the FRP reinforcement ratio ρ_f. This paper examines the effects of these six parameters on the ductility performance of CY beams. As CY beams are significantly different from conventional flexural members, a numerical study is first undertaken to examine the characteristics of the CY beams. The general behavior of CY beams is subsequently investigated through an analytical study.

* Corresponding author. Tel.: +852 27844259; fax: +852 27887612.
E-mail address: yfwu00@cityu.edu.hk (Y.F. Wu).

0958-9465/$ - see front matter © 2009 Elsevier Ltd. All rights reserved.
doi:10.1016/j.cemconcomp.2009.06.007

Nomenclature

A	area enclosed by the moment–curvature response curve
A_f	area of the FRP reinforcement
A_n	area inside the moment–curvature curve, see Fig. 11
A_s	area of the steel reinforcement
A_w	area outside the moment–curvature curve, see Fig. 11
b	width of beam
d	effective depth of beam
E_b	elastic modulus of CY block
E_c	elastic modulus of concrete
E_c'	tangent modulus of concrete in Mander's model
E_f	elastic modulus of FRP
E_s	elastic modulus of steel bar
E_{sec}	secant modulus of concrete in Mander's model
F_b	resultant force of CY block
F_{bmi}	resultant force of CY block at maximal FRP strain state
F_c	resultant force of concrete
F_{cmi}	resultant force of concrete at maximal FRP strain state
F_{fi}	resultant force of FRP at maximal strain state
F_s	resultant force of steel reinforcement
f_b	strength of CY block
f_c	compressive strength of concrete
$M_{\max}$	moment at peak point of moment–curvature curve
M_m	moment at maximal FRP strain
N_b	number of discretized layers of CY block
N_c	number of discretized layers of compression concrete
n	ratio of ε_{cu} to ε_0
PDM	percentage drop in moment from maximal strain state to failure state
R_c	curvature ratio by Eq. (15)
R_m	curvature ratio by Eq. (13)
R_y	curvature ratio by Eq. (14)
Z_{bi}	lever arm of CY block resultant force at maximal FRP strain state
Z_{ci}	lever arm of concrete resultant force at maximal FRP strain state
α_i	ratio of compression force contributed by CY block at maximal FRP strain state
β_i	factor by Eq. (A4)
δ_{ci}	factor of FRP strain at complete crushing of concrete over maximal strain
δ_M	limit of moment drop, defined as 15% in this paper
δ_{ui}	strain relaxation factor from maximal strain state to failure state
δ_{yi}	ratio of FRP strain at failure of CY block over maximal FRP strain state
ε_{by}	yielding strain of CY block
ε_{bu}	ultimate strain of CY block
ε_{cmi}	strain at extreme compression fiber of concrete at maximal FRP strain
ε_{cu}	crushing strain of concrete
ε_{fm}	maximal strain limit of FRP
ε_{fu}	ultimate strain of FRP
ε_{fui}	strain of FRP at cross-sectional failure
ε_{sy}	yield strain of steel reinforcement
ε_0	concrete strain at peak stress
ε_1	transition strain between Cases I and II
ε_2	transition strain between Cases II and III
φ_y	curvature ductility
γ_i	ratio of compression force contributed by concrete at maximal FRP strain state
η	ratio of height of CY block to depth of beam
κ_{cci}	curvature at complete crushing of concrete immediately below CY block
κ_{cyi}	curvature at complete yielding of CY block
κ_{emi}	equivalent curvature at maximal FRP strain state give by Eq. (A3)
$\kappa_{\max}$	curvature at peak point of moment–curvature curve
κ_{mi}	curvature at maximal FRP strain state
κ_{ui}	ultimate curvature of CY section
κ_y	yield curvature
ρ_f	FRP reinforcement ratio
ρ_s	compression steel reinforcement ratio
ζ	distance from centroid of steel reinforcement to top fiber of beam divided by d

Subscript

i	1, 2 and 3 for Cases I, II and III, respectively, as defined in Fig. 13

2. Assumptions and stress–strain relationships

For simplicity, the following assumptions are adopted in the present work: (1) plane sections remain plane; (2) the tensile strength of concrete is neglected; (3) the CY block material is elastic-perfectly plastic (Fig. 2); and (4) the stress–strain curve of concrete is approximated by a triangular model (Fig. 3a). Based on existing experimental evidence, the elastic-perfectly plastic model shown in Fig. 2 is a good approximation for several CY materials [7,10,11]. Fig. 3a is also adequate for the purpose of the present study; this adequacy is later verified by comparing results based on this simple model with those based on the more sophisticated model of Mander et al. [12] (Fig. 3b). The compression steel is assumed to be elastic-perfectly plastic while the FRP is assumed to be linearly elastic.

3. Numerical study

The numerical model for the moment–curvature relationship of a typical cross-section is based on the conventional layered meth-

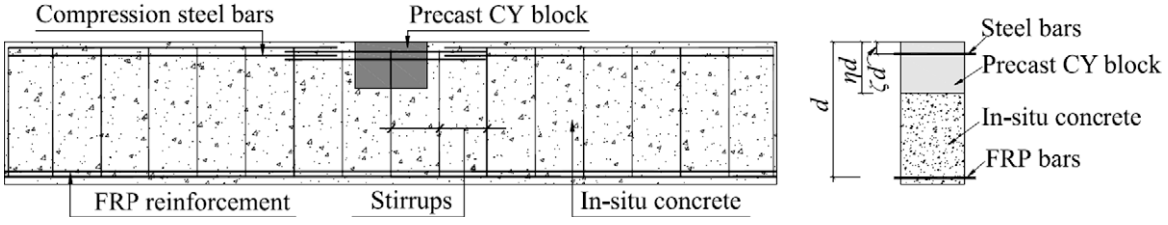

Fig. 1. Structural configuration of an RC beam with a compression-yielding block.

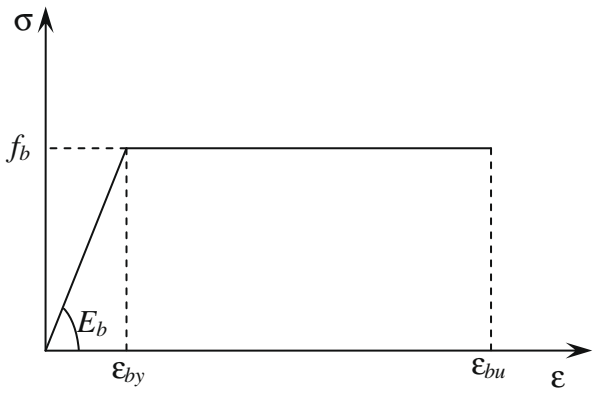

Fig. 2. Stress–strain relationship of a CY material.

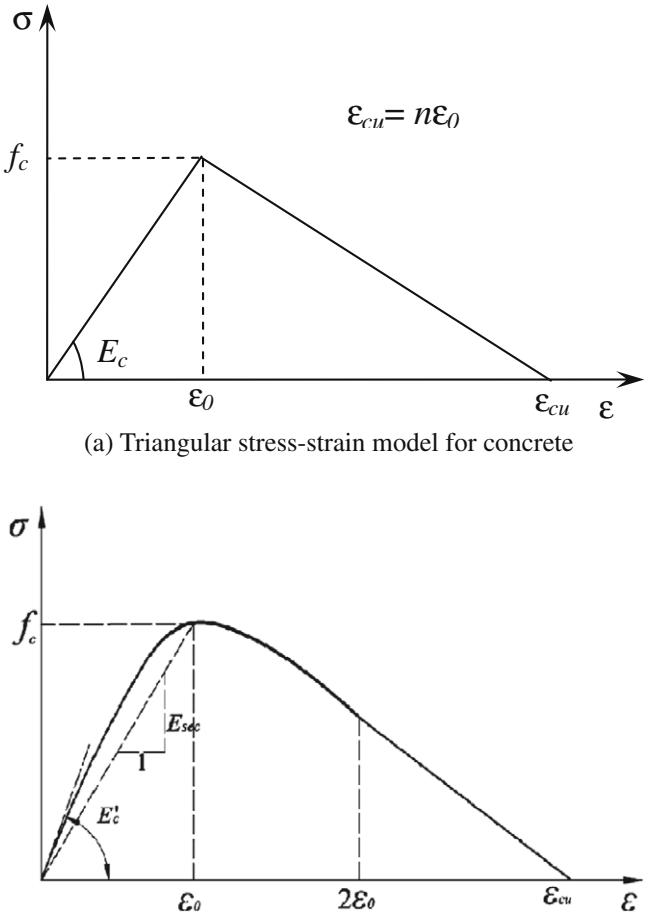

Fig. 3. Stress–strain model for concrete in compression.

od [13] where the section is discretized into many layers and the strain of each layer is evaluated at its centre for a given curvature. The neutral axis for a given curvature is calculated by considering the equilibrium of the section based on the assumed stress–strain relationships, and the corresponding moment is then obtained by integration of the moment contribution by individual layers (force times the corresponding lever arm). A typical discretized section and the strain distribution are shown in Fig. 4.

A typical 180 mm wide by 350 mm deep section (d = 300 mm) was selected in the numerical study. The material properties were

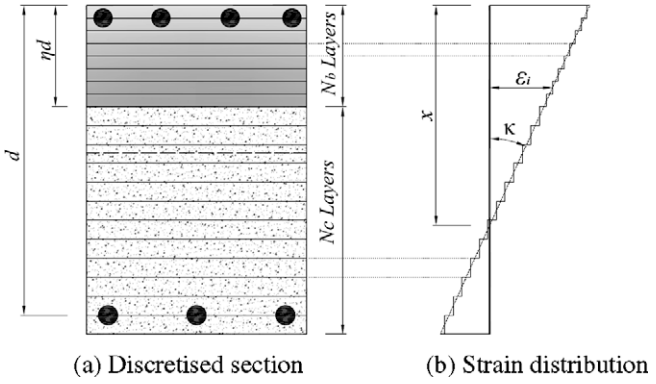

Fig. 4. Discretisation of cross-section.

assumed to be as follows: concrete compressive strength f_c = 30 MPa; concrete strain at peak stress ε_0 = 0.002; concrete crushing strain ε_{cu} = 0.006; elastic modulus of FRP E_f = 124 GPa; rupture strain of FRP ε_{fu} = 0.017; elastic modulus of steel bars E_s = 200 GPa; yield strain of steel bars ε_{sy} = 0.0015; and the location ratio of the steel bars (Fig. 1) ζ = 0.1. The ultimate strain of the CY block ε_{bu} was set to be 20% in this part of the study, based on the experimental investigations of various CY blocks. The numerical results are presented in Figs. 5–10. In each figure, the values of one or two parameters vary within a certain range but the other parameters are fixed at certain values that are shown in the figures. The numerical results were produced using a computer program developed in the present study. These results allow the following observations to be made:

(1) Effect of the CY block depth ηd – the degradation of moment resistance after the peak point reduces as η increases (Fig. 5). However, the yield curvature also increases at the same time. Therefore, there exists an optimum value of η at which the ductility is maximized; this value is about 0.5 for the present example section. In Fig. 5, the FRP reinforcement ratio is fixed. As η increases, the maximum strain experienced by the FRP $\varepsilon_{f\max}$ increases and approaches the rupture strain. If the amount of FRP reinforcement falls below the current one or the CY block strength is higher, the structure will fail due to FRP rupture. Therefore, if brittle FRP rupture

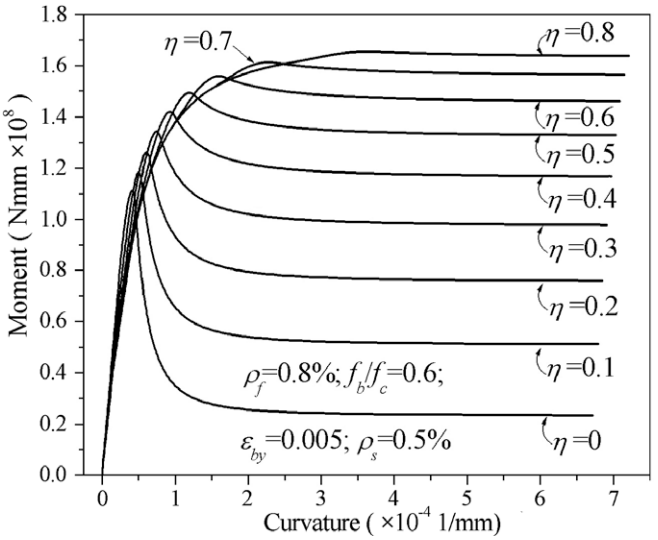

Fig. 5. Moment–curvature responses for ρ_f = 0.8%.

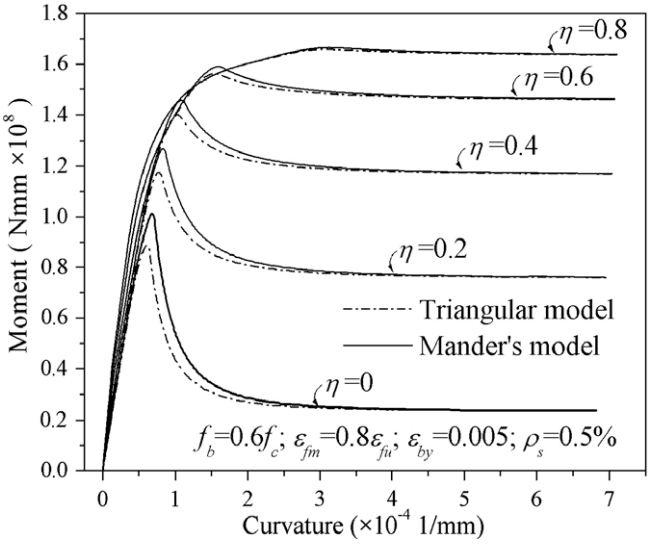

Fig. 6. Moment–curvature responses for $\varepsilon_{fm} = 0.8\varepsilon_{fu}$.

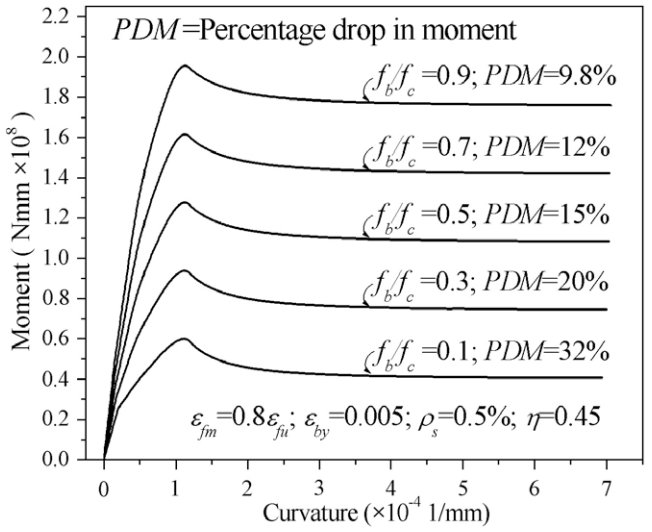

Fig. 7. Effects of strength of CY block.

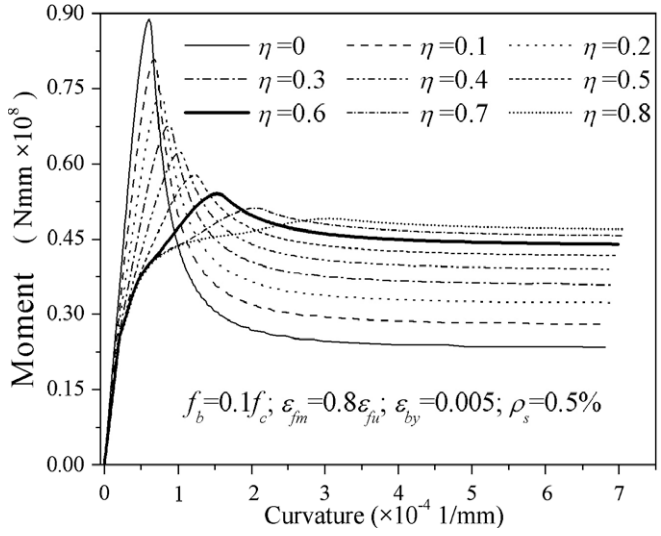

Fig. 8. Moment–curvature responses for $f_b/f_c = 0.1$.

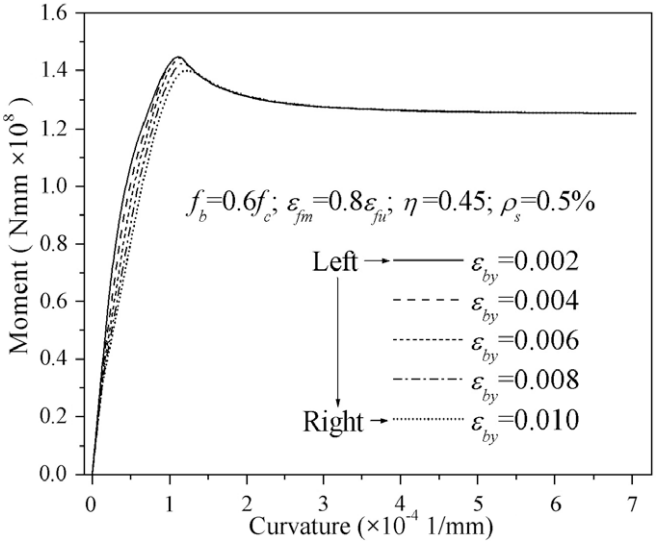

Fig. 9. Effects of elastic modulus of CY block.

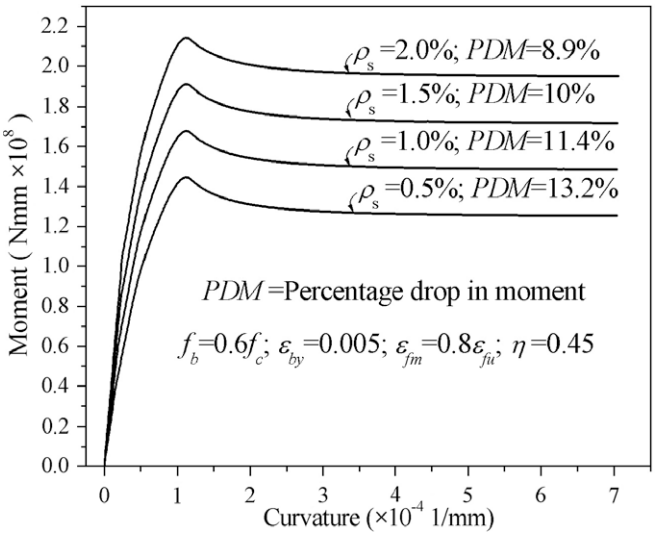

Fig. 10. Effects of compression steel reinforcement ratio ρ_s.

failure is to be avoided in such a beam, a limit must be imposed on the maximal strain allowed in the FRP and such a limit can be realized by varying the FRP reinforcement ratio. On the other hand, in order to make efficient use of the FRP material, the allowable maximum FRP strain should not be too small. For these reasons, the quantity of FRP is not further examined as a variable in the subsequent discussions. Instead, this ratio was determined in such a way that the maximum strain experienced by the FRP is equal to 80% of the FRP rupture strain, or $\varepsilon_{fm} = 0.8\varepsilon_{fu}$. Under this condition, the effect of η on the moment–curvature response is shown in Fig. 6, which is similar to that seen in Fig. 5. There is also an optimal size of the CY block in terms of ductility, at a similar value between 0.4 and 0.6.

(2) In Fig. 6, it can be seen that the moment capacity increases slightly when Mander's stress–strain model is used instead of the triangular stress–strain model for concrete, since the area below the stress–strain curve of Mander's model is larger than that of the triangle model. However, the difference

is small and the trend of the curves and the initial rigidity are almost identical. Thus these two models lead to little difference in the predicted response of CY beams. For simplicity, the triangular model was used in all other numerical simulations and in the analytical study.

(3) Effect of the CY block strength f_b/f_c – when the relative strength of the CY block f_b/f_c increases, the percentage drop in moment (*PDM*) in the descending branch becomes smaller, and hence the ductility of the section increases, as shown in Fig. 7. The rigidity of the section also increases with the strength of the CY block. However, this observation does not mean that a weak CY block cannot lead to a ductile response. When η is equal to 0.6, a weak CY block still leads to a ductile response, as shown in Fig. 8, although both the moment capacity and the section rigidity are lower than those in Fig. 7. Therefore, for each value of f_b/f_c, there is a certain value of η at which the ductility is maximized. This will be further illustrated by the analytical study presented later in the paper.

(4) Effect of the CY block yield strain ε_{by} – Fig. 9 shows that the rigidity of a CY beam before the peak point reduces with an increase of the yield strain ε_{by} but this yield strain increase has little effect on the softening branch of the curve. As a result, a lower yield strain or a higher stiffness of CY block leads to greater ductility.

(5) Effect of the compression steel ratio ρ_s – as shown in Fig. 10, a larger reinforcement ratio results in a smaller reduction in the moment after the peak strength, as well as a greater moment capacity and greater rigidity. Therefore, the ductility of a CY beam may increase slightly with an increase in the compression steel reinforcement ratio ρ_s.

4. Analytical study

In this section, an analytical study of the moment–curvature response of CY sections is presented to gain further insight into the ductility performance of CY beams.

4.1. Definition of curvature ductility

There are many different definitions of ductility in the literature. The ductility definition that is based on energy equivalence is adopted in this work, as shown in Fig. 11. The curvature κ_y is the yield curvature of an equivalent bi-linear response curve which encloses an area equal to that of the actual moment–curvature curve, i.e.

$$A_w = A_n, \tag{1}$$

which leads to

$$\kappa_{\max} M_{\max} - \kappa_y M_{\max}/2 = A, \tag{2}$$

or

$$\kappa_y = 2(\kappa_{\max} - A/M_{\max}), \tag{3}$$

where $\kappa_{\max}$ and $M_{\max}$ are the curvature and moment at the peak of the actual response curve, respectively; and A is the area enclosed by the moment–curvature response curve up to the peak point.

Therefore, the curvature ductility is given by

$$\varphi_y = \frac{\kappa_u}{\kappa_y} = \frac{\kappa_u}{2(\kappa_{\max} - A/M_{\max})}, \tag{4}$$

in which κ_u is the ultimate curvature of the CY beam. The enclosed area A can be evaluated by the integration of the moment–curvature response curve, i.e.

$$A = \int_0^{\kappa_{\max}} M(\kappa) d\kappa. \tag{5}$$

4.2. Moment–curvature relationship

The moment–curvature relationship of a typical CY section can be derived analytically using the conventional reinforced concrete theory [14,15] incorporating appropriate stress–strain models for the constituent materials. However, the derivation of this relationship is complicated due to the bi-linear stress–strain models of the constituent materials, which requires different equations for different ranges of strain. The values of the various parameters also affect the application of different equations as well as their combinations; e.g. the CY block may or may not completely yield when the concrete below the CY block reaches the descending branch of the stress–strain relationship. Based on a rational analysis of the deformation process, three typical moment–curvature response curves are shown in Fig. 12. Seven turning points (A–G) that correspond to the qualitative changes of the constituent materials are indicated on the response curve. For mild steel, the yield strain is usually smaller than that of the CY block, therefore the moment–curvature response is linear elastic up to the yielding of the steel bars (point A). Thereafter the moment–curvature response enters

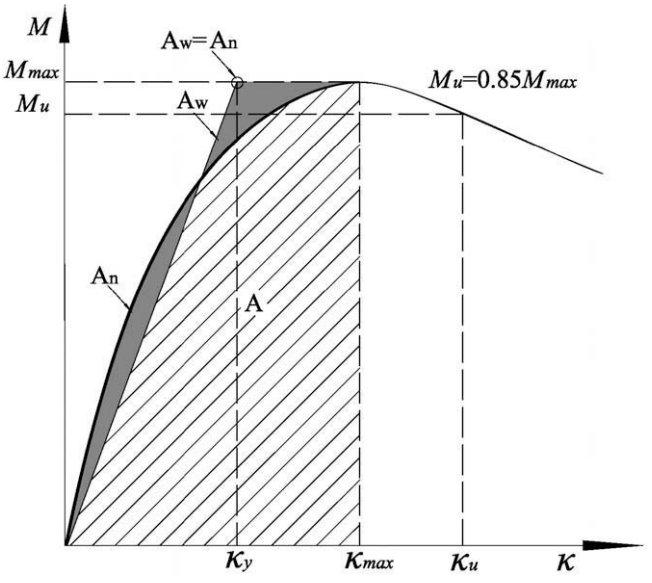

Fig. 11. Definition of curvature ductility.

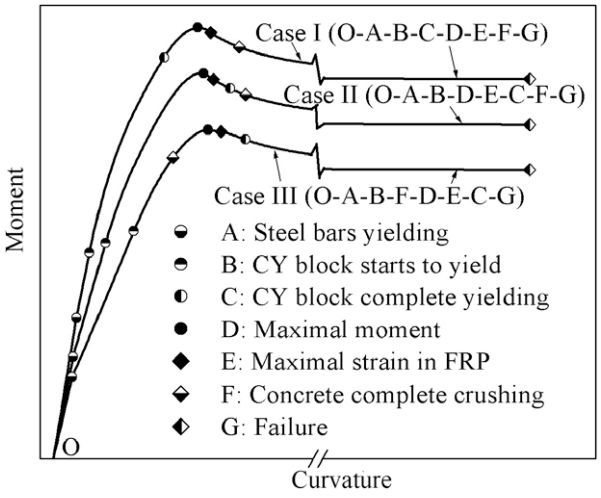

Fig. 12. Moment–curvature responses and their turning points.

into a nonlinear and inelastic phase experiencing the yielding process of the CY block (from point B to C), the peak point of the response (point D), the attainment of the maximal strain in the FRP (called the maximal strain state, point E), the complete crushing of concrete (point F), and finally the complete failure (point G). For each stage of deformation, analytical expressions can be derived.

Point E is a critical point in this study and it can be derived from the following equation:

$$\frac{dF_f}{d\kappa} = 0, \tag{6}$$

where κ is the curvature and F_f is the force in the FRP bars which is given by

$$F_f = F_s + F_c + F_b, \tag{7}$$

in which F_s, F_c, and F_b are the resultant forces of the steel bars, concrete and the CY block, respectively, all being functions of κ. Due to the difference in the attainment of points C, E and F (Fig. 12), the three possible stress profiles at the onset of the maximum FRP strain are shown in Fig. 13. For each case, different expressions are needed to calculate the internal forces in Eq. (7). Solving Eq. (6) leads to the following results:

$$\varepsilon_{cm1} = \sqrt{\varepsilon_{fm}^2 + 2\varepsilon_{cu}\varepsilon_{fm} + \varepsilon_{cu}^2/n} - \varepsilon_{fm} \quad \text{for Case I,} \tag{8}$$

$$\varepsilon_{cm2} = \sqrt{\frac{f_c(\varepsilon_{fm}+\varepsilon_{cu})^2/(\varepsilon_{cu}-\varepsilon_0) + E_b(\varepsilon_{fm}+\varepsilon_{by})^2 - f_c\varepsilon_{cu}}{f_c/(\varepsilon_{cu}-\varepsilon_0)+E_b}} - \varepsilon_{fm} \quad \text{for Case II,} \tag{9}$$

$$\varepsilon_{cm3} = \sqrt{(\varepsilon_{fm}+\varepsilon_{by})^2 - \varepsilon_{cu}f_c/E_b} - \varepsilon_{fm} \quad \text{for Case III,} \tag{10}$$

where ε_{cm1}, ε_{cm2}, and ε_{cm3} are the strain values of the extreme compression fiber (top fiber) of the concrete at the onset of the maximum FRP strain ε_{fm} for Case I, II and III, respectively.

Based on Fig. 13, Eq. (8) is applicable when $\varepsilon_{by} \leqslant \varepsilon_{cm1} \leqslant \varepsilon_{cu}$; Eq. (9) should be used when $\varepsilon_{cm2} < \varepsilon_{by}$ and $\varepsilon_{cm2} < \varepsilon_{cu}$; and Eq. (10) is applicable when $\varepsilon_{cu} \leqslant \varepsilon_{cm3} \leqslant \varepsilon_{by}$. These three conditions are equivalent to $\varepsilon_{by} \leqslant \varepsilon_1$ for Case I; $\varepsilon_1 < \varepsilon_{by} < \varepsilon_2$ for Case II; and $\varepsilon_{by} \geqslant \varepsilon_2$ for Case III, where

$$\varepsilon_1 = \sqrt{\varepsilon_{fm}^2 + 2\varepsilon_{cu}\varepsilon_{fm} + \varepsilon_{cu}^2/n} - \varepsilon_{fm}, \tag{11}$$

$$\varepsilon_2 = \sqrt{(\varepsilon_{cu}+\varepsilon_{fm})^2 + \varepsilon_{cu}f_c/E_b} - \varepsilon_{fm}. \tag{12}$$

Therefore, ε_1 and ε_2 are the two boundary strains of ε_{by} that divides the response into three cases as shown in Fig. 13.

Based on Eqs. (8)–(10), the analytical expressions for the four critical points C, E, F and G can be derived. Detailed derivations and results are given in the Appendix A.

4.3. Three useful curvature ratios

To facilitate the following discussions of the moment–curvature response of CY beams, the following three curvature ratios are defined:

$$R_m = \frac{\kappa_{ui}}{\kappa_{mi}}, \tag{13}$$

$$R_y = \frac{\kappa_{ui}}{\kappa_{cyi}}, \tag{14}$$

$$R_c = \frac{\kappa_{ui}}{\kappa_{cci}}, \tag{15}$$

where i = 1, 2, or 3 for Cases I, II and III, respectively; R_m is the ratio of the ultimate curvature κ_{ui} to the peak curvature κ_{mi}; R_y is the ratio of the ultimate curvature κ_{ui} to the curvature at the onset of complete yielding of the CY block κ_{cyi}; and R_c is the ratio of the ultimate curvature κ_{ui} to the curvature at the onset of complete crushing of concrete immediately below the CY block κ_{cci}. Analytical solutions for κ_{ui}, κ_{cyi}, and κ_{cci} are derived in the Appendix A.

5. Ductility performance of CY beams

The ductility performance of CY beams is discussed in this section using the analytical equations derived in Section 4. The same cross-section investigated in the numerical simulations is further considered in this section.

5.1. Effect of CY block size and strength

Fig. 14 shows the effect of the depth ratio η on curvature ductility φ_y. It is noted that there is an optimum size for the CY block to maximize the ductility of the section when other variables have fixed values. It can also be seen that the optimum size of the CY block is almost identical regardless of whether a maximum strain limit is imposed on the FRP reinforcement (which results in a variable FRP quantity for different η values) or a fixed FRP reinforcement ratio is used.

Moreover, the trend of variation of the curvature ratio R_m is identical to that of the curvature ductility φ_y; and both of them reach their maximum at the same value of η. This conclusion is always correct and the reason is simple: both the R_m and φ_y curves have an ascending branch that is governed by the 15% moment

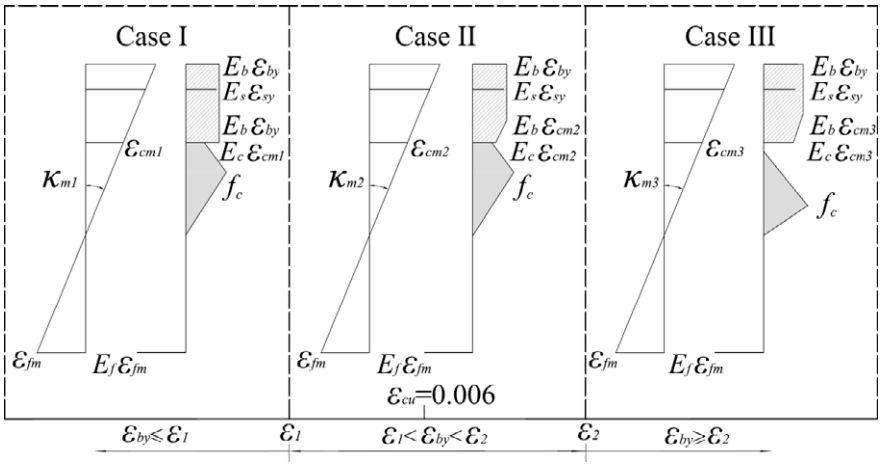

Fig. 13. Stress and strain profiles for three distinct cases.

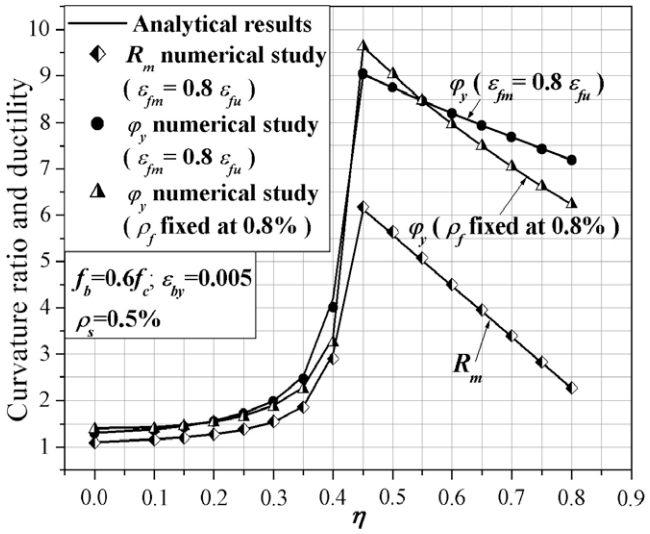

Fig. 14. Curvature ratio and ductility vs. η.

drop and a descending branch that is governed by the onset of the ultimate strain in the CY block, and the peaks are the points of intersection of the ascending and descending branches that signify the coincidence of the 15% moment drop and the onset of the ultimate CY strain. For a given CY section, there can be only one η value at which the 15% moment drop and the onset of the ultimate CY strain occur simultaneously. This observation is very useful that can greatly simplify the optimal design of the CY section, because the calculation of R_m is much simpler than that of φ_y. Therefore, the optimal η can be calculated directly from Eq. (A14) in Appendix A by letting *PDM* = 15% (or another value if the failure point is defined as another percentage of drop in moment).

The discrete points in Fig. 14 were obtained from numerical simulations, and were calculated from the peak point of the moment–curvature curve (point D) instead of the attainment of the maximum FRP strain (point E). The close agreement between the numerical results and the analytical results (shown by solid lines) provides a mutual validation of the analytical model and the numerical model, and also indicates the little difference that exists between point E and point D.

Fig. 15 depicts the influence of the strength of the CY block f_b on curvature ductility. When a maximum strain limit is imposed on the FRP, the curvature ductility increases with the CY block strength until a certain point after which any further increase in strength has little effect. However, when a fixed reinforcement ratio is imposed instead, the curvature ductility reduces after attaining a maximum value; in other words, a single optimum value of f_b exists.

Figs. 14 and 15 show that for a given f_b/f_c value, an optimum value of η exists at which the curvature ductility is maximized, and vice versa.

5.2. Effect of the elastic modulus (or yielding strain) of CY block

Fig. 16 shows the influence of the elastic modulus of a CY block on ductility. It is noted that a reduction in the elastic modulus of the CY block reduces both the curvature ductility φ_y and the curvature ratio R_y but has little effect on the curvature ratio R_c. The curvature ratio R_m remains constant up to point P_A, and then reduces gradually towards point P_B before it decreases further. The two points P_A and P_B in Fig. 16 are the critical points that divide the analytical results into three Cases (I–III); the corresponding strains at these two points are the critical strain ε_1 and ε_2 as given by Eqs. (11) and (12), respectively. As R_m depends on the path of the descending branch from the peak point to the ultimate failure point, a constant value indicates that the elastic modulus of the CY block does not affect the descending branch before ε_{by} reaches ε_1, which is also illustrated in Fig. 9. At point P_A, the curve for R_y intersects with the curve for R_m; in other words, the attainment of the complete yielding of the CY block coincides with the attainment of the FRP maximum strain. This is exactly the case at the transition point from Case I to Case II in Fig. 13. At point P_B, the curve for R_c intersects with the curve for R_m; in other words, the complete crushing of concrete immediately below the CY block occurs when the FRP maximum strain is reached. This is the transition point between Case II and Case III shown in Fig. 13. Apart from these two transition points, the complete yielding of the CY block, the complete crushing of concrete immediately below the

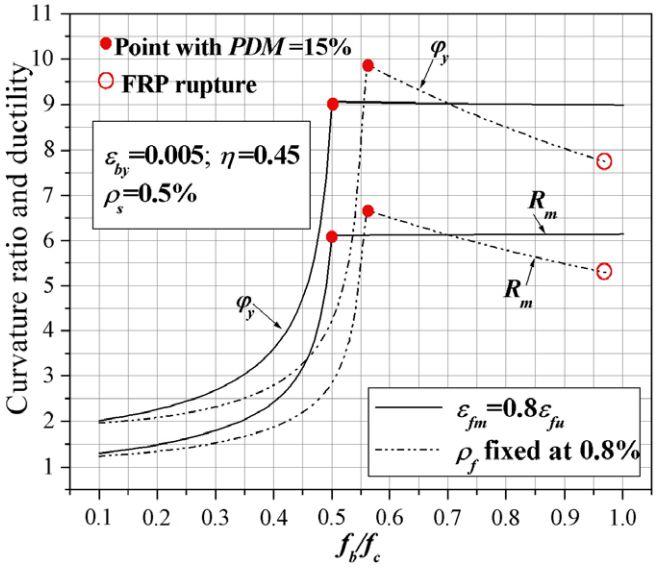

Fig. 15. Curvature ratio and ductility vs. strength of CY block.

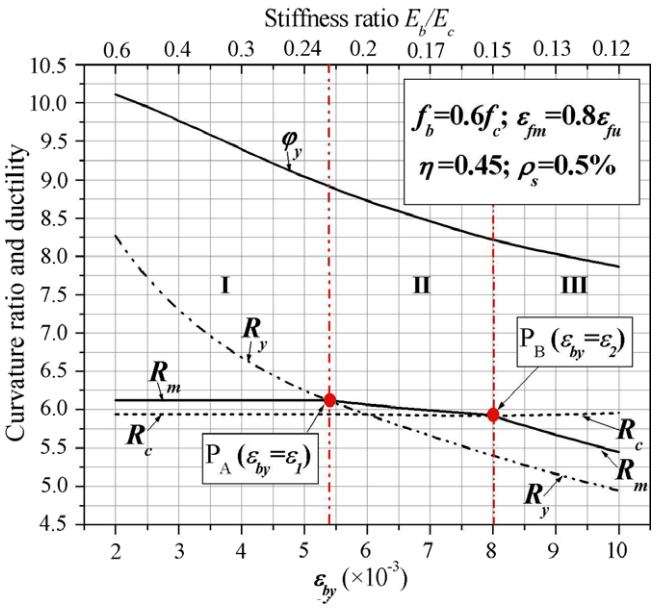

Fig. 16. Effects of elastic modulus of CY block on ductility.

CY block and the attainment of the maximum FRP strain occur at different times. The results shown in Fig. 16 provide a clear exposition of the need for the case divisions adopted in the analytical study from a different perspective.

5.3. Effect of the ultimate strain of the CY block

It is clearly seen in Fig. 17 that the ductility of CY beams is directly proportional to the ultimate strain of the CY block ε_{bu} when failure is governed by its ultimate strain (failure mode I). However, the ultimate strain of the CY block has no effect on ductility once failure is governed by the percentage drop in moment (failure mode II), as shown by the dash–dotted line in the figure. The two failure modes are defined in the Appendix A.

5.4. Effect of the steel reinforcement ratio

Fig. 18 depicts the influence of the steel reinforcement ratio ρ_s on the ductility of a CY section. It is seen that the curvature ductility φ_y increases slightly with the amount of steel reinforcement. This is due to the increase in the rigidity of the CY section, which can also be seen in Fig. 10. Therefore, the inclusion of a greater amount of steel reinforcement in the CY block enhances the ductility, rigidity and moment capacity of a CY section. Of course, this conclusion is based on the assumption that a maximum strain control is imposed on the FRP; in other words, when the compression steel is increased in the CY block, the amount of FRP will be increased in a corresponding manner. However, the use of a large amount of compression steel for ductility enhancement is not a desirable solution, because it requires a significant corresponding increase in the amount of FRP but the resulting ductility enhancement is very limited (Fig. 18). If a significant amount of compression steel is used in a CY block, especially for the purpose of increasing the moment capacity of the section, adequate restraint must be provided to avoid the buckling of the steel bars and the consequent rapid degradation in the compressive resistance of the CY block.

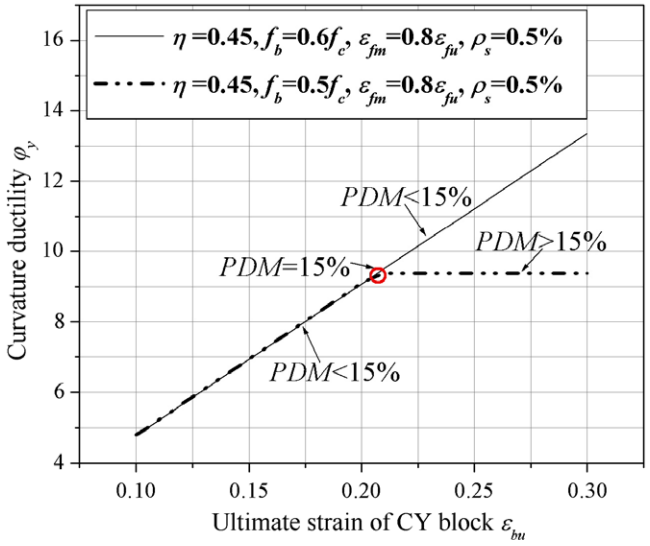

Fig. 17. Effects of ultimate strain of CY block on ductility.

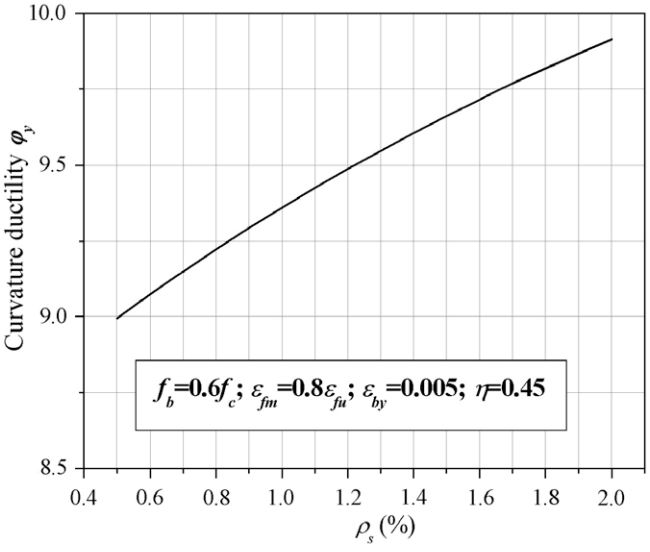

Fig. 18. Effects of compression steel reinforcement ratio on ductility.

6. Summary and conclusions

This paper has examined the ductility behavior of compression-yielding (CY) reinforced concrete (RC) beams using both numerical and analytical approaches. The key parameters were first identified and their effects on the curvature ductility of CY beams were then investigated. A method of design for the maximum possible amount of ductility of a CY beam with a given FRP reinforcement ratio (or a given CY block size or strength) has been presented. The relationships among the CY block strength, the section moment resistance and the section rigidity of a CY beam were also revealed. The main conclusions that arise from the results and discussions presented in this paper are as follows:

1. The use of a compression-yielding block can greatly increase the ductility of RC beams reinforced with non-ductile reinforcement.
2. For a given CY block strength, there is an optimum size of the CY block and a corresponding FRP reinforcement ratio that maximize the ductility of the section. Similarly when the size of the CY block is fixed, an optimal value of the CY block strength and a corresponding FRP reinforcement ratio exist, at which the ductility of the section is maximized.
3. The optimal η can be calculated directly from Eq. (A14) by letting $PDM = \delta_M$, where δ_M is the maximum allowable percentage drop in moment.
4. A stiffer CY block and a higher compression steel reinforcement ratio are both beneficial to the ductility, rigidity and moment capacity of a CY beam.

Acknowledgment

The work described in this paper was fully supported by a Grant from the Research Grants Council of the Hong Kong Special Administrative Region, China [Project No.: CityU 122106].

Appendix A. Analytical solutions for critical points

A.1. Peak response (point D or E)

At the onset of the maximal FRP strain (point E), the curvature κ_m, the maximal tensile force of FRP F_f and the corresponding moment M_m can be derived based on Eqs. (8)–(10) and Fig. 13, which gives

$$\kappa_{mi} = \frac{\varepsilon_{fm} + \varepsilon_{cmi}}{(1-\eta)d}, \tag{A1}$$

$$F_{fi} = E_s \varepsilon_{sy} \rho_s bd + (1-\beta_i) E_b \varepsilon_{by} \eta bd + \frac{b\varepsilon_{cu} f_c}{2\kappa_{emi}}, \tag{A2}$$

where the subscript $i = 1, 2, 3$ stands for Case I, II and III, respectively; b and d are the width and the effective depth of the concrete beam, respectively; ρ_s is compression steel reinforcement ratio; E_s and ε_{sy} are the modulus and yielding strain of the steel bars, respectively; and κ_{emi} and β_i are given by

$$\kappa_{emi} = \frac{\kappa_{mi}}{1 - \frac{n}{n-1}\left(1 - \frac{\varepsilon_{cmi}}{\varepsilon_{cu}}\right)^2} \quad (\text{for } i = 1,2), \tag{A3-1}$$

$$\kappa_{em3} = \kappa_{m3} \quad (\text{for } i = 3), \tag{A3-2}$$

$$\beta_1 = 0 \quad (\text{for } i = 1), \tag{A4-1}$$

$$\beta_i = \frac{(\varepsilon_{by} - \varepsilon_{cmi})^2 (1-\eta)}{2\eta\varepsilon_{by}(\varepsilon_{fm} + \varepsilon_{cmi})} \quad (\text{for } i = 2,3). \tag{A4-2}$$

The FRP reinforcement ratio ρ_f corresponding to the maximum allowable FRP strain ε_{fm} is given by

$$\rho_f = F_f / E_f \varepsilon_{fm} bd. \tag{A5}$$

Based on the sectional equilibrium, the corresponding moment M_m can be obtained from Fig. 13 as

$$M_{mi} = F_{fi}[\alpha_i Z_{bi} + (1 - \alpha_i - \gamma_i)(1-\zeta)d + \gamma_i Z_{ci}], \tag{A6}$$

where ζ is the ratio of the distance relative to d from the centroid of steel bars to the top fiber of the beam (see Fig. 1); Z_{ci} and Z_{bi} are the lever arms of the concrete and CY block resultant forces, respectively, as given by

$$Z_{ci} = \left[1 - \frac{3n\varepsilon_0\varepsilon_{cmi}^2 - \varepsilon_{cmi}^3 - 3n\varepsilon_0^2\varepsilon_{cmi} + n\varepsilon_0^3}{(\varepsilon_{fm} + \varepsilon_{cmi})(6n\varepsilon_{cmi}\varepsilon_0 - 3\varepsilon_{cmi}^2 - 3n\varepsilon_0^2)}\right](1-\eta)d \quad (\text{for } i = 1,2), \tag{A7-1}$$

$$Z_{c3} = \frac{3n\varepsilon_{fm} + (n+1)\varepsilon_{cu}}{3n(\varepsilon_{fm} + \varepsilon_{cm3})}(1-\eta)d \quad (\text{for } i = 3), \tag{A7-2}$$

$$Z_{b1} = \left(1 - \frac{\eta}{2}\right)d \quad (\text{for } i = 1), \tag{A8-1}$$

$$Z_{bi} = \left[1 - \frac{\eta}{2} - \frac{3\varepsilon_{fm} + 2\varepsilon_{cmi} + \varepsilon_{by}}{3(\varepsilon_{fm} + \varepsilon_{cmi})}(1-\eta)\beta_i\right]\frac{d}{1-\beta_i} \quad (\text{for } i = 2,3), \tag{A8-2}$$

and the two characteristic ratios α_i and γ_i are defined by

$$\alpha_i = \frac{F_{bmi}}{F_{fi}} = \frac{(1-\beta_i)\varepsilon_{by} E_b \eta}{E_s\varepsilon_{sy}\rho_s + (1-\beta_i)E_b\varepsilon_{by}\eta + \varepsilon_{cu} f_c/(2d\kappa_{emi})}, \tag{A9}$$

$$\gamma_i = \frac{F_{cmi}}{F_{fi}} = \frac{\varepsilon_{cu} f_c/(2d\kappa_{emi})}{E_s\varepsilon_{sy}\rho_s + (1-\beta_i)E_b\varepsilon_{by}\eta + \varepsilon_{cu} f_c/(2d\kappa_{emi})}, \tag{A10}$$

where F_{bmi} and F_{cmi} are the resultant forces of the CY block and the concrete at the maximal FRP strain, respectively.Strictly speaking, the point at the onset of the maximal FRP strain (point E) is different from the point of maximal moment resistance (point D) for FRP-reinforced concrete beams. However, engineering experience has shown that the onset of maximal tensile force is very close the occurrence of the peak moment. This can also be seen in the numerical results in Section 4 and the results of the analytical study in Section 5. For simplicity, the moment M_m is treated as the maximal moment of the moment–curvature response curve for evaluation of ductility in this work, with negligible loss of accuracy of the results.

A.2. Failure state (point G)

The ultimate curvature κ_u in Eq. (4) depends on the failure modes that are classified into two types:

1. Failure mode I – CY block failure. The ultimate failure is governed by the attainment of the ultimate strain ε_{bu} in the CY block, i.e. the strain at the top fiber of CY block reaches the ultimate value of ε_{bu}. Thus, the ultimate curvature κ_u is defined as the curvature at the failure of the CY block.
2. Failure mode II – the moment resistance after the peak drops below the allowable limit before the CY block failure, i.e. $PDM \geqslant \delta_M$ at CY block failure. In this case, the ultimate curvature κ_u is defined as the curvature at the onset of $PDM = \delta_M$.

Based on the above definition, the analytical expressions of κ_u corresponding to the two failure modes are separately derived in the following sections.

A.2.1. Failure mode I

For failure mode I, the failure is due to the attainment of the ultimate strain at the top fiber. In this case, the percentage drop in moment (PDM) is smaller than δ_M, and the ultimate curvatures in the aforementioned three cases can be, respectively, expressed as

$$\kappa_{ui} = \frac{\varepsilon_{bu} + \varepsilon_{fui}}{d}. \tag{A11}$$

The corresponding strain in the FRP at the failure point, ε_{fui}, can be written as

$$\varepsilon_{fui} = (1 - \delta_{ui})\varepsilon_{fm}, \tag{A12}$$

where δ_{ui} is the FRP strain relaxation factor after the maximum strain point. Since the loss of the FRP strain is due to the drop of the resultant force in the compression concrete, the strain relaxation factor is derived to be

$$\delta_{ui} = \frac{1}{2}\left[\gamma_i - \frac{\alpha_i\beta_i}{1-\beta_i} + \frac{\varepsilon_{bu}}{\varepsilon_{fm}} + 1 - \sqrt{(\gamma_i - \frac{\alpha_i\beta_i}{1-\beta_i} + \frac{\varepsilon_{bu}}{\varepsilon_{fm}} + 1)^2 - 4\left(\gamma_i - \frac{\alpha_i\beta_i}{1-\beta_i}\right)\left(\frac{\varepsilon_{bu}}{\varepsilon_{fm}} + 1\right) + 4\gamma_i\frac{\kappa_{emi}}{\varepsilon_{fm}}d}\right]. \tag{A13}$$

As the CY block has fully yielded after the peak resistance, the drop of moment after the peak is due to concrete crushing. Thus, the percentage drop in moment (PDM) can be evaluated as

$$PDM = \frac{\Delta M}{M} = \frac{C_{i3}\alpha_i + C_{i4}\gamma_i}{C_{i0} + C_{i1}\alpha_i + C_{i2}\gamma_i}, \tag{A14}$$

where

$$C_{i0} = 1 - \zeta, \tag{A15}$$

$$C_{i1} = \frac{1}{1-\beta_i}\left[\beta_i - \eta/2 - \frac{3\varepsilon_{fm} + 2\varepsilon_{cmi} + \varepsilon_{by}}{3(\varepsilon_{fm} + \varepsilon_{cmi})}(1-\eta)\beta_i\right] + \zeta, \tag{A16}$$

$$C_{i2} = Z_{ci}/d - (1-\zeta), \tag{A17}$$

$$C_{i3} = 0 \quad (\text{for } i = 1), \tag{A18-1}$$

$$C_{i3} = -\frac{\beta_i}{1-\beta_i}\frac{3\varepsilon_{fm} + 2\varepsilon_{cmi} + \varepsilon_{by}}{3(\varepsilon_{fm} + \varepsilon_{cmi})}(1-\eta) \quad (\text{for } i = 2,3), \tag{A18-2}$$

$$C_{i4} = Z_{ci}/d - \frac{\kappa_{emi}[3n(1-\delta_{ui})\varepsilon_{fm} + (n+1)\varepsilon_{cu}]}{3n[\varepsilon_{bu} + (1-\delta_{ui})\varepsilon_{fm}]^2}d. \tag{A19}$$

A.2.2. Failure mode II

For failure mode II, the ultimate curvature occurs at the point where the moment drop is at the maximal allowable level δ_M, or

$$\frac{M_m - M_{uII}}{M_m} = \delta_M, \tag{A20}$$

and

$$\sum N_{uII} = 0, \tag{A21}$$

where M_{uII} is the moment of the failure point and can be derived from the sectional equilibrium; N_{uII} is correspondingly total axial force of the section.

Solving Eqs. (A20) and (A21) yields the ultimate curvature κ_u for failure mode II

$$\kappa_u = \kappa_{ui} = \sqrt[3]{\frac{Q_i}{2}+\sqrt{\left(\frac{Q_i}{2}\right)^2-\left(\frac{P_i}{3}\right)^3}}+\sqrt[3]{\frac{Q_i}{2}-\sqrt{\left(\frac{Q_i}{2}\right)^2-\left(\frac{P_i}{3}\right)^3}}, \tag{A22}$$

where

$$Q_i = \frac{\kappa_{emi}^2\gamma_i^2\varepsilon_{fm}}{(1-\delta_M)\gamma_i Z_{ci} - \alpha_i\delta_M Z_{b\delta i} - \delta_M(1-\alpha_i-\gamma_i)(1-\zeta)d}, \tag{A23}$$

$$P_i = \frac{\kappa_{emi}\gamma_i\left[(1-\gamma_i)\varepsilon_{fm}+\frac{n+1}{3n}\varepsilon_{cu}\right]}{(1-\delta_M)Z_{ci} - \alpha_i\delta_M Z_{b\delta i} - \delta_M(1-\alpha_i-\gamma_i)(1-\zeta)d}, \tag{A24}$$

and

$$Z_{b\delta i} = \frac{1}{1-\beta_i}\left[1-\frac{\eta}{2}-\frac{3\varepsilon_{fm}+2\varepsilon_{cmi}+\varepsilon_{by}}{3(\varepsilon_{fm}+\varepsilon_{cmi})}(1-\eta)\beta_i\left(1-\frac{1}{\delta_M}\right)\right]d. \tag{A25}$$

A.3. Complete yielding of CY block and complete crushing of concrete (points C and F)

Complete yielding of the CY block and complete crushing of concrete immediately below the CY block are the other two critical points in terms of the response of CY beams. The axial force contribution of the CY block remains constant after its complete yielding while the concrete stress gradually reduces to zero at its top fiber. The corresponding curvature κ_{cy} at complete yielding of CY block (point C) can be derived with the same method as that for the curvature κ_u for failure mode I, leading to

$$\kappa_{cyi} = \frac{\varepsilon_{by}+(1-\delta_{yi})\varepsilon_{fm}}{(1-\eta)d}, \tag{A26}$$

where δ_{yi} is strain variation ratio of FRP relative to the maximum FRP strain

$$\delta_{yi} = \frac{1}{2}\left[\gamma_i - \frac{\alpha_i\beta_i}{1-\beta_i}+\frac{\varepsilon_{by}}{\varepsilon_{fm}}+1 - \sqrt{\left(\gamma_i-\frac{\alpha_i\beta_i}{1-\beta_i}+\frac{\varepsilon_{by}}{\varepsilon_{fm}}+1\right)^2 - 4\left(\gamma_i-\frac{\alpha_i\beta_i}{1-\beta_i}\right)\left(\frac{\varepsilon_{by}}{\varepsilon_{fm}}+1\right)+4\gamma_i\frac{\omega_i\kappa_{emi}}{\varepsilon_{fm}}(1-\eta)d}\right], \tag{A27}$$

in which

$$\omega_1 = 1, \quad (\text{for } i=1) \tag{A28}$$

$$\omega_i = \begin{cases} 1-\frac{n}{n-1}\left(1-\frac{\varepsilon_{by}}{\varepsilon_{cu}}\right)^2 & \text{if } \varepsilon_{by} < \varepsilon_{cu} \\ 1 & \text{if } \varepsilon_{by} \geqslant \varepsilon_{cu} \end{cases} \quad (\text{for } i=2,3). \tag{A29}$$

The curvature κ_{cc} at complete crushing of concrete (point F) is similarly derived as

$$\kappa_{cc1} = \frac{\varepsilon_{cu}+(1-\delta_{c1})\varepsilon_{fm}}{(1-\eta)d} \quad (\text{for } i=1), \tag{A30-1}$$

$$\kappa_{cc2} = \begin{cases} \frac{\varepsilon_{cu}+(1-\delta_{c2})\varepsilon_{fm}}{(1-\eta)d} & \text{if } \varepsilon_{by} < \varepsilon_{cu} \\ \left(B_c+\sqrt{B_c^2+4A_cC_c}\right)\Big/2A_c & \text{if } \varepsilon_{by} \geqslant \varepsilon_{cu} \end{cases} \quad (\text{for } i=2), \tag{A30-2}$$

$$\kappa_{cc3} = \left(B_c+\sqrt{B_c^2+4A_cC_c}\right)\Big/2A_c \quad (\text{for } i=3), \tag{A30-3}$$

where δ_{c1} and δ_{c2} are strain variation ratio of FRP relative to the maximum FRP strain at the corresponding state, which can be expressed as

$$\delta_{ci} = \frac{1}{2}\left[\gamma_i - \frac{\alpha_i\beta_i}{1-\beta_i}+\frac{\varepsilon_{cu}}{\varepsilon_{fm}}+1 - \sqrt{\left(\gamma_i-\frac{\alpha_i\beta_i}{1-\beta_i}+\frac{\varepsilon_{cu}}{\varepsilon_{fm}}+1\right)^2 - 4\left(\gamma_i-\frac{\alpha_i\beta_i}{1-\beta_i}\right)\left(\frac{\varepsilon_{cu}}{\varepsilon_{fm}}+1\right)+4\gamma_i\frac{\kappa_{emi}}{\varepsilon_{fm}}(1-\eta)d}\right], \tag{A31}$$

and

$$A_c = E_fA_f(1-\eta)d, \tag{A32}$$

$$B_c = E_b\varepsilon_{by}\eta bd + \varepsilon_{cu}E_fA_f + E_sA_s\varepsilon_{sy}, \tag{A33}$$

$$C_c = [\varepsilon_{cu}bf_c - (\varepsilon_{by}-\varepsilon_{cu})^2E_bb]/2. \tag{A34}$$

where A_f and A_s are, respectively, the area of the FRP and steel reinforcement.

References

[1] Benmokrane B, Chaallal O, Masmoudi R. Flexural response of concrete beams reinforced with FRP reinforcing bars. ACI Struct J 1996;91(2):46–55.
[2] Pecce M, Manfredi G, Cosenza E. Experimental response and code models of GFRP RC beams in bending. J Compos Constr ASCE 2000;4(4):182–90.
[3] Gravina RJ, Smith ST. Flexural behaviour of indeterminate concrete beams reinforced with FRP bars. Eng Struct 2008;30(9):2370–80.
[4] Vijay PV, GangaRao HVS. Bending behavior and deformability of glass fiber-reinforced polymer reinforced concrete members. ACI Struct J 2001;98(6):834–42.
[5] Naaman AE. FRP reinforcements in structural concrete: assessment, progress and prospects. In: Proceeding of the sixth international symposium on FRP reinforcement for concrete structures. Singapore: World Scientific; 2003. p. 1–24.
[6] Wu YF. Improving the ductility of reinforced concrete members reinforced with FRP bars. In: Proceeding of 2nd fib congress, Naples, Italy, June 508; 2006 [ID 10-48].
[7] Wu YF. Ductility demand of compression yielding FRP-reinforced concrete beams. ACI Struct J 2008;105(1):104–10.
[8] Wu YF. New avenue of achieving ductility for reinforced concrete members. J Struct Eng ASCE 2006;132(9):1502–6.
[9] Huang Y, Wu YF. Ductility of hybrid fiber reinforced concrete. In: Proceeding of international symposium on innovation & sustainability of structures in civil engineering (ISISS'2005), Nanjing, China, November 20–22; 2005. p. 2314–26.
[10] Liu K, Wu YF. Compression yielding by SIFCON block for FRP-reinforced concrete beams. In: Proceeding of first Asia-Pacific conference on FRP in structures, Hong Kong, China, December 12–14; 2007.
[11] Liu XC, Wu YF, Leung AYT, Hou JG. Mechanical behavior of mild steel compressive yielding blocks. In: Proceeding of first Asia-Pacific conference on FRP in structures, Hong Kong, China, December 12–14; 2007.
[12] Mander JB, Priestley MJN, Park R. Theoretical stress-strain model for confined concrete. J Struct Eng ASCE 1988;114(8):1804–26.
[13] Wu YF. Rational definition of the flexural deformation capacity of RC column sections. Eng Struct 2004;26:641–50.
[14] Paulay T, Priestley MJN. Seismic design of reinforced concrete and masonry buildings. New York: Wiley; 1992.
[15] Nilson AH, Darwin D, Dolan CW. Design of concrete structures. Boston: McGraw Hill; 2003.